Supporting Information

Fe-modified $Co_2Mo_3O_8$ promoted nitrate cascade reduction reaction coupled with oxygen evolution reaction for electrocatalytic ammonia synthesis

Yaru Wang, Shiyu Qin, Xiaoyue Chen, Xiangchao Meng and Zizhen Li *

Key Laboratory of Marine Chemistry Theory and Technology (Ministry of Education), College of Chemistry & Chemical Engineering, Ocean University of China, Qingdao, Shandong, 266100, China.

* Corresponding author. Email: lizizhen@ouc.edu.cn

S1. Experimental section

S1.1 Chemicals

Ammonium molybdate tetrahydrate ($H_{24}Mo_7N_6O_{24}\cdot 4H_2O$), iron (III) nitrate nonahydrate ($Fe(NO)_3\cdot 9H_2O$) were purchased from Shanghai Aladdin Biochemical Technology Co., Ltd. Cobalt nitrate hexahydrate ($Co(NO_3)_2\cdot 6H_2O$) was purchased from Shanghai Macklin Biochemical Co., Ltd. Potassium hydroxide (KOH) and hydrochloric acid (HCl) were purchased from Sinopharm Chemical Reagent Co., Ltd. Potassium nitrate (KNO_3) and acetone (CH_3COCH_3) were purchased from Xilong Scientific Co., Ltd. Ni foams (NF) were purchased from Kunshan Guangjiayuan New Materials Co. Ltd. None of the chemicals were further decontaminated.

S1.2 Synthesis of catalysts

Synthesis of FeCoMo/NF precursors: FeCoMo/NF precursors were synthesized by a simple hydrothermal method. Firstly, 2 cm × 3 cm nickel foam (NF) was sequentially immersed in 0.2 M HCl, acetone, and deionized water respectively for 10 minutes of ultrasonication for pre-treatment to remove the oxidized layer and organics on the surface of NF. Subsequently, 250 mg $H_{24}Mo_7N_6O_{24}\cdot 4H_2O$, 235 mg $Co(NO_3)_2\cdot 6H_2O$, and 163 mg $Fe(NO)_3\cdot 9H_2O$ were dispersed into 40 mL deionized water with continuous stirring for 30 minutes. The well-mixed solution was transferred to a 50 mL Teflon-lined autoclave (Anhui Kemi Instrument Co., Ltd, China). Thereafter, the pretreated NF was placed vertically in the reactor and maintained at 150 °C for a period of 6 hours. Subsequently, the catalysts were cooled to room temperature and rinsed with deionized water and ethanol in alternating sequences. This was followed by drying at 80 °C for 4 hours to obtain the FeCoMo/NF precursor.

Synthesis of FeCoMo/NF: The FeCoMo/NF catalysts were synthesized by rapid Joule heating under an Ar/H_2 atmosphere. A 1 cm × 1.5 cm FeCoMo/NF precursor was positioned in the centre of a graphite plate, which was subsequently assembled in the

Joule heating device cavity (Hefei in situ technology Co., Ltd. China). Subsequently, the cavity of the device was evacuated to exclude air interference with the catalyst. FeCoMo/NF was obtained by treating the catalyst at 800 °C for 90 seconds under an Ar/H_2 gas stream atmosphere.

Synthesis of CoMo/NF and Mo/NF: For comparison, CoMo/NF and Mo/NF catalysts were synthesized using the same simple hydrothermal and rapid Joule heating methods. CoMo/NF catalysts were synthesized without the addition of $Fe(NO)_3 \cdot 9H_2O$, while Mo/NF catalysts were synthesized without the addition of $Fe(NO)_3 \cdot 9H_2O$ and $Co(NO_3)_2 \cdot 6H_2O$.

S1.3 Characterizations

Scanning electron microscopy (SEM) images and energy dispersive X-ray (EDS) elemental mapping images were obtained by the Czech TESCAN MIRA LMS instrument. Transmission electron microscopy (TEM) images and high-resolution transmission electron microscopy (HRTEM) images were obtained using a JEM-2100PLUS transmission electron microscope. X-ray diffraction (XRD) and X-ray photoelectron spectroscopy (XPS) were collected by Bruker-D8 Advance and Thermo Scientific K-Alpha, respectively. The C 1s peak at 284.80 eV was used as an energy reference for all binding energies. Ultraviolet-visible (UV-vis) absorption spectra were collected by a Persee TU-1901 dual-beam UV-vis spectrophotometer.

S1.4 Electrochemical measurements

Electrochemical measurements of NO_3RR: All electrochemical tests were performed on a CHI660E electrochemical workstation (CH Instrument, Ins., China). A three-electrode system comprising a Hg/HgO as the reference electrode, a carbon rod as the counter electrode, and an electrocatalyst (1 cm × 1 cm) as the working electrode was employed for the NO_3RR test in an H-type cell. Before electrochemical testing, the cathode and anode chambers of the H-type cell were filled with 30 mL of 0.1 M KOH

with 1000 $mg_{NO_3^-}$/L electrolyte. This was followed by the introduction of 30 min of Ar gas into the cathode chamber, to remove dissolved nitrogen and oxygen from the cathode solution. The working electrode was subjected to 50 cyclic voltammetry tests at a scan rate of 50 mV/s to activate the working electrode. Subsequently, the chronoamperometry tests were tested for 0.5 h at a stirring rate of 300 r.p.m. under a series of applied constant potentials. LSV curves were obtained at a sweep rate of 5 mV/s in the range of -0.6 to -1.6 V *vs.* Hg/HgO. The electrochemically active surface area (ECSA) of the catalysts was calculated from the capacitance of the electrostatic double-layer capacitor (C_{dl}) according to the following equation: $ECSA = A \times C_{dl}/C_s$, where A is the geometrical area of the catalysts (cm^2) and C_s is the specific capacitance of the catalyst (0.04 mF cm^{-2}). Furthermore, cyclic voltammetry (CV) tests were conducted at varying sweep speeds (5 to 25 mV/s) to obtain C_{dl} values. Electrochemical impedance spectroscopy (EIS) tests were performed at open-circuit potential within the frequency range of 10^5 to 10^{-2} Hz. All potentials were converted with the reversible hydrogen electrode (RHE) as a reference, utilizing the following formula: E (*vs.* RHE) = E (*vs.* Hg/HgO) + 0.098 + 0.0591 × pH. All tests were performed at room temperature.

Electrochemical measurements of OER: The OER tests were carried out in a single chamber cell in a three-electrode system using Hg/HgO as the reference electrode, a carbon rod as the counter electrode, and an electrocatalyst (1 cm × 1 cm) as the working electrode. The electrolyte consisted of a solution of 0.1 M KOH with 1000 $mg_{NO_3^-}$/L. LSV tests were obtained at a sweep rate of 10 mV/s in the range of 0 to 1.0 vs. Hg/HgO with 80% iR compensation.

Electrochemical measurements of NO_3RR-OER: For the H-type cell, FeCoMo/NF catalyst was used as the cathode and anode, and the two-electrode NO_3RR-OER coupling reaction was carried out at a stirring rate of 300 r.p.m. Whereas for the flow cell, the FeCoMo/NF catalyst was used as the cathode and anode for the two-electrode NO_3RR-OER coupling reaction at 60% of the maximum flow rate.

S1.5 Determination

Determination of NH_3: The indophenol blue method was used for the detection of NH_3 in the electrolyte. Firstly, 2 mL of a 1 M sodium hydroxide solution containing 5 wt.% salicylic acid and 5 wt.% sodium citrate was added to 2 mL of electrolyte solution diluted to the detection limit. Subsequently, 1 mL of a 0.05 M sodium hypochlorite solution and 0.2 mL of a 1 wt.% sodium nitroprusside solution were added and mixed well. After standing for 2 hours at ambient temperature, the mixtures were detected using a Persee TU-1901 dual-beam UV-vis spectrophotometer at a wavelength of 655 nm. The Nessler's reagent was also used for further detection of NH_3 in the electrolyte. The Nessler's reagent and detection equipment were provided by Beijing Lianhua YongXing Science and Technology Development Co. Ltd.

Determination of NO_2^-: The Griess method was used for the detection of NO_2^- in the electrolyte. Firstly, 0.2 g of N-(1-naphthyl) ethylenediamine dihydrochloride, 4.0 g of sulfanilamide, and 10 mL of phosphoric acid were dispersed homogeneously into 50 mL of deionized water to configure the Griess reagent. Subsequently, 0.1 mL of Griess reagent was added to 5 mL of electrolyte solution diluted to the detection limit and mixed well. After standing for 20 minutes at ambient temperature, the mixtures were detected using a Persee TU-1901 dual-beam UV-vis spectrophotometer at a wavelength of 540 nm.

Determination of NO_3^-: For the determination of NO_3^-, 0.1 mL of 1M HCl and 10 uL of 0.8% sulfamic acid solution were sequentially added to 5 mL of electrolyte solution diluted to the detection limit and mixed well. A Persee TU-1901 dual-beam UV-vis spectrophotometer was used to record the absorbance intensities at 220 nm and 275 nm. The intensity of the absorption peak $A_{NO_3^-}$ was linearly related to the concentration of NO_3^- where $A_{NO_3^-} = A_{220\ nm} - A_{275\ nm}$.

S1.6 Calculation

The Faradaic efficiency (FE) is calculated as follows:

$$FE = (n \times F \times C \times V)/(M \times Q) \quad \text{S1}$$

The yield rate is calculated as follows:

$$\text{Yield rate} = (C \times V)/(M \times t \times A) \quad \text{S2}$$

where F represents the Faradaic constant (96500 C mol^{-1}); C represents the concentration of the substance in the cathode chamber; V represents the volume of electrolyte in the cathode chamber; M represents the molecular mass of the substance; Q represents the total of charge that actually pass through the working electrode during the reaction; A represents the geometric area of the catalyst; t represents the reaction time.

The half-cell energy efficiency (EE) for ammonia synthesis is calculated as follows:

$$EE = (1.23 - E_0)FE_{NH_3}/(1.23 - E) \quad \text{S3}$$

The full-cell energy efficiency (EE) for ammonia synthesis is calculated as follows:

$$EE = (1.23 - E_0)FE_{NH_3}/\text{Voltage} \quad \text{S4}$$

E_0 represents the equilibrium potential for the conversion of nitrate to ammonia (0.69 V), FE_{NH_3} represents the Faraday efficiency of NH_3, 1.23 V is the equilibrium potential for the oxidation of water (assuming that the overpotential for the oxidation of water is zero), and E (*vs.* RHE) is the applied potential.

The electrical power consumption (EPC) in the two-electrode system represents the amount of electrical energy (usually expressed in kWh) required to produce 1 kg of product, calculated as follows:

$$EPC = (\text{Voltage} \times n \times F)/(FE_{NH_3} \times M) \quad \text{S5}$$

Where n is the number of transferred electrons (n=8).

S1.7 DFT calculations

All calculations were performed using density functional theory (DFT), implemented in the Vienna ab initio Simulation Package (VASP), and the electron-ion interactions

were handled using the projector augmented wave (PAW) potential. The generalized gradient approximation (GGA) of Perdew-Burke-Ernzerhof (PBE) was employed to deal with electron exchange and correlation. The plane wave cut-off energy was 400 eV and simulations were performed on a 1×3×1 k-point grid. The calculations were carried out using an energy convergence criterion within 10^{-5} and a vacuum thickness of 15 Å along the z-direction to ensure that inter-plate interactions were ignored.

S2. Figures

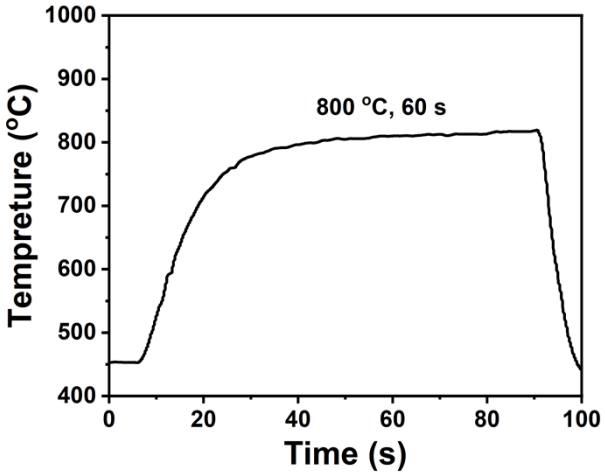

Fig. S1 Real-time temperature graph of synthetic FeCoMo/NF.

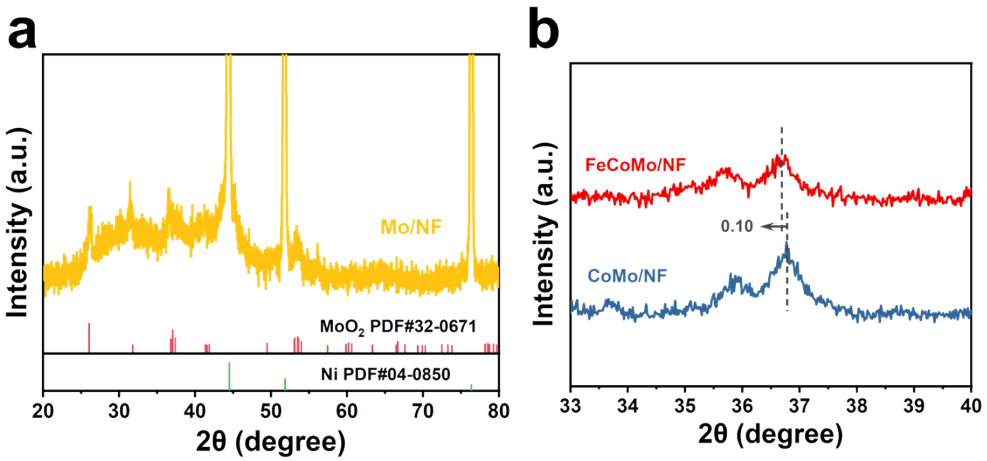

Fig. S2 (a) XRD pattern of Mo/NF. (b) Enlarged XRD pattern of FeCoMo/NF catalyst.

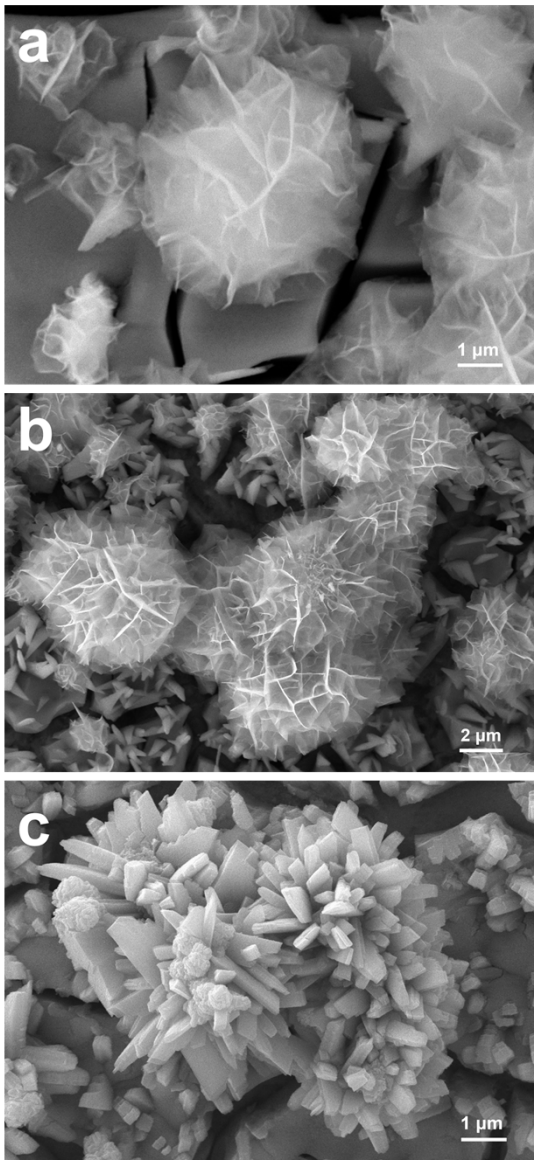

Fig. S3 SEM images of (a) FeCoMo/NF precursor, (b) FeCoMo/NF, and (c) CoMo/NF.

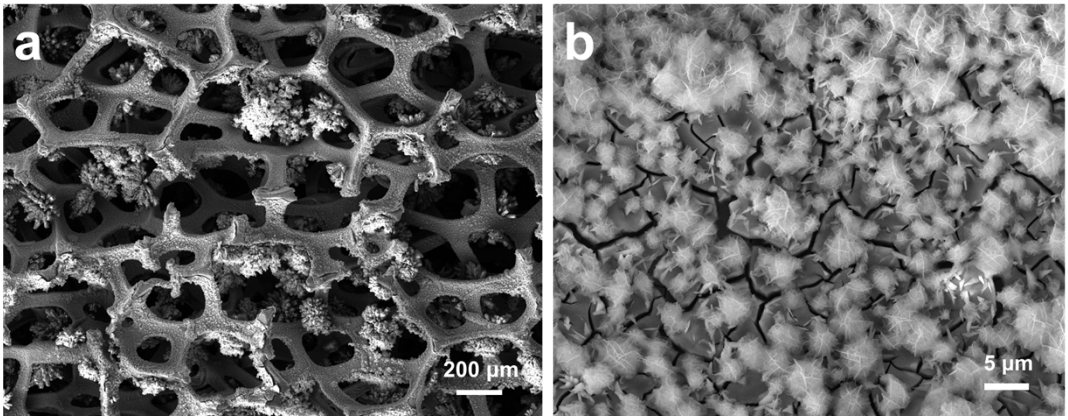

Fig. S4 SEM images of FeCoMo/NF.

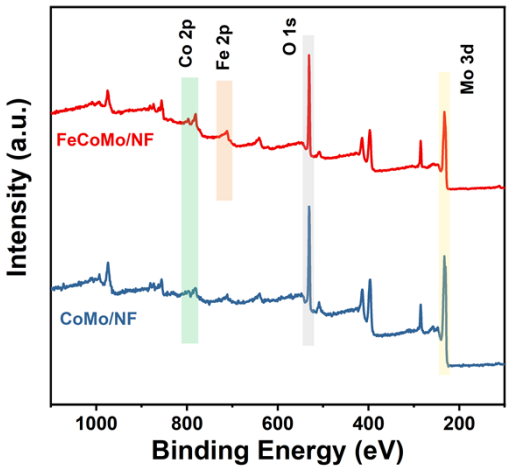

Fig. S5 XPS spectra of FeCoMo/NF and CoMo/NF catalysts.

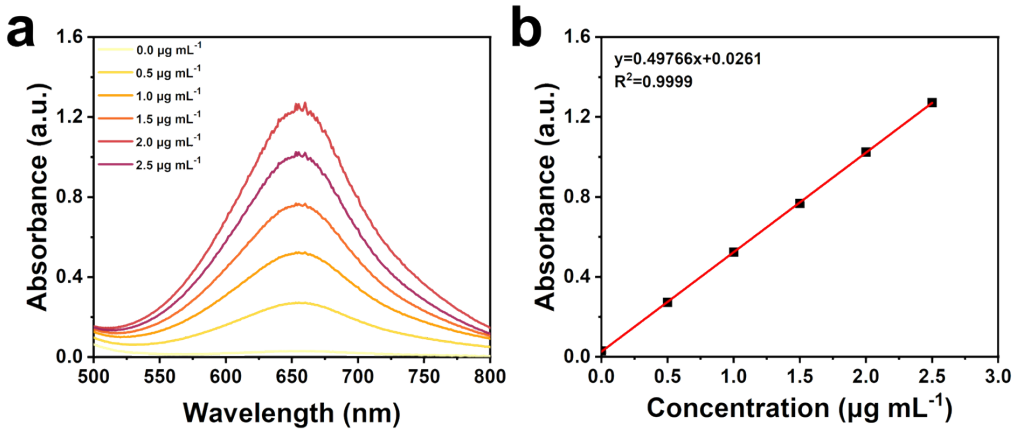

Fig. S6 (a) UV-vis spectra of various ammonia concentrations. (b) Standard curve for the quantitative determination of ammonia.

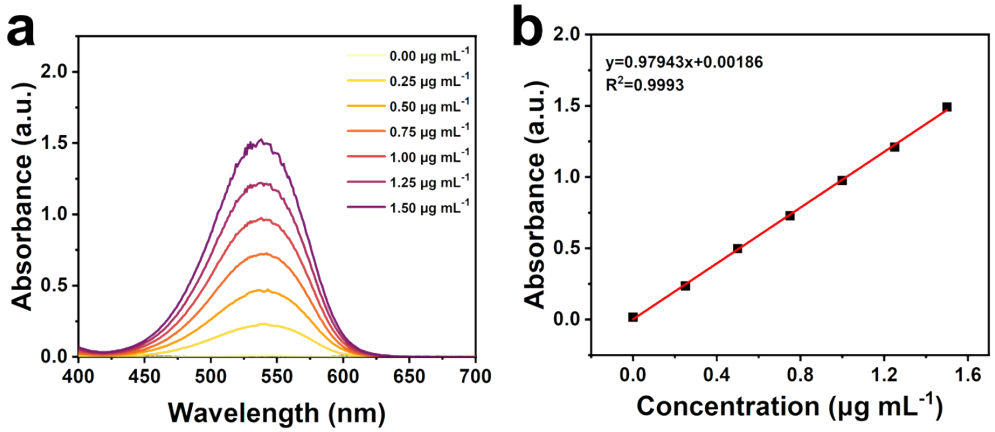

Fig. S7 UV-vis spectra of different nitrite concentrations. (b) Standard curve for quantitative determination of nitrite.

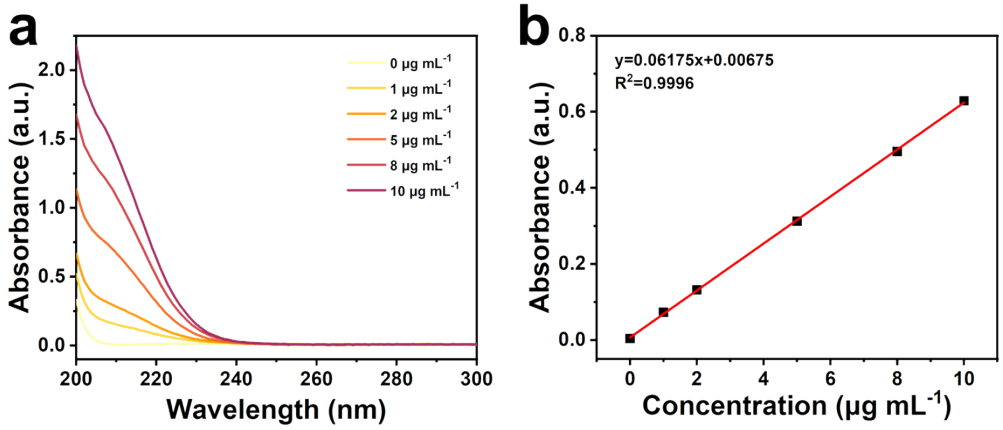

Fig. S8 (a) UV-vis spectra of different nitrate concentrations. (b) Standard curve for the quantitative determination of nitrate.

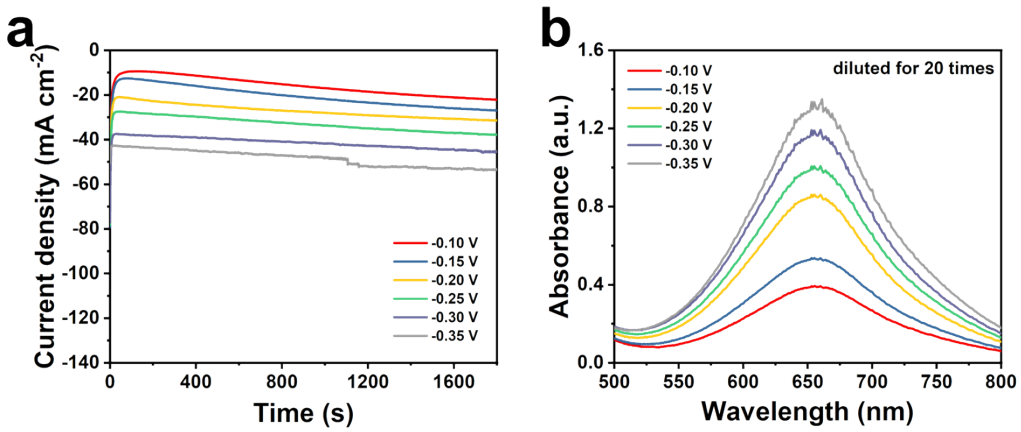

Fig. S9 (a) Chronoamperometry curves and (b) the corresponding UV-vis absorption spectra of FeCoMo/NF at various potentials in 0.1 M KOH with 1000 $mg_{NO_3^-}$/L.

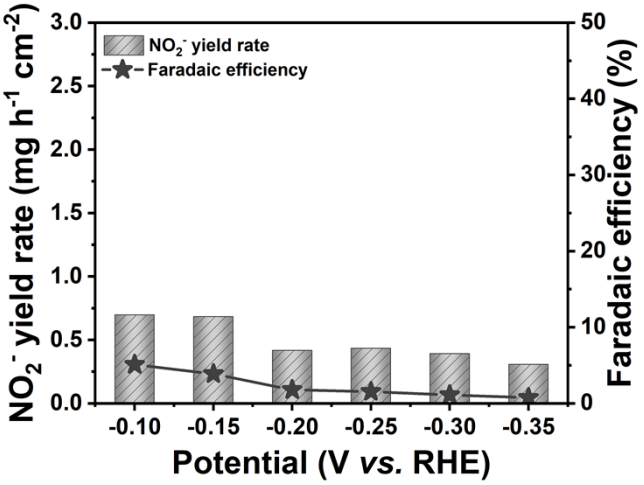

Fig. S10 NO_2^- yield rate and Faradaic efficiency of FeCoMo/NF at varying potentials.

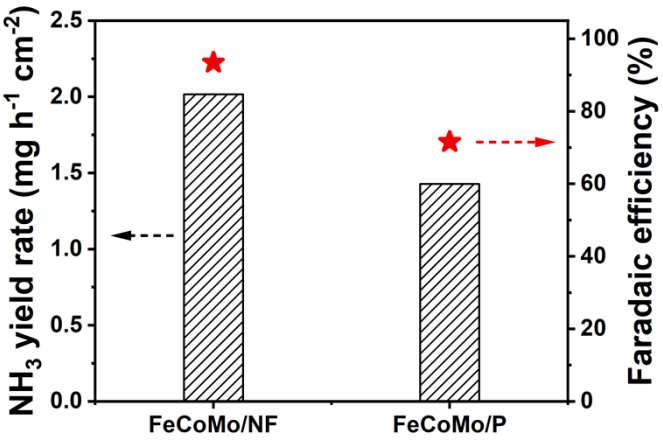

Fig. S11 NO_3RR performance of FeCoMo/NF and FeCoMo/P.

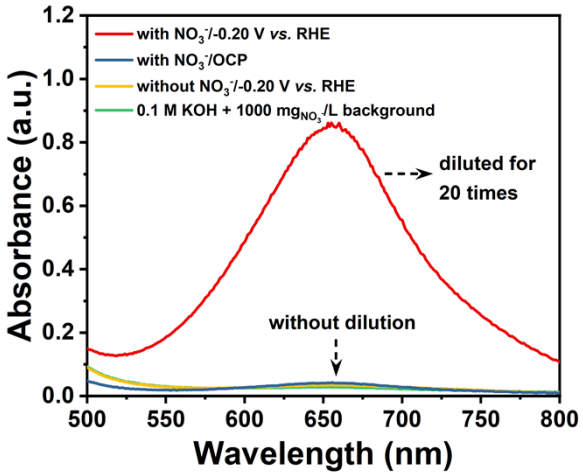

Fig. S12 UV-vis absorption spectrums of blank control group.

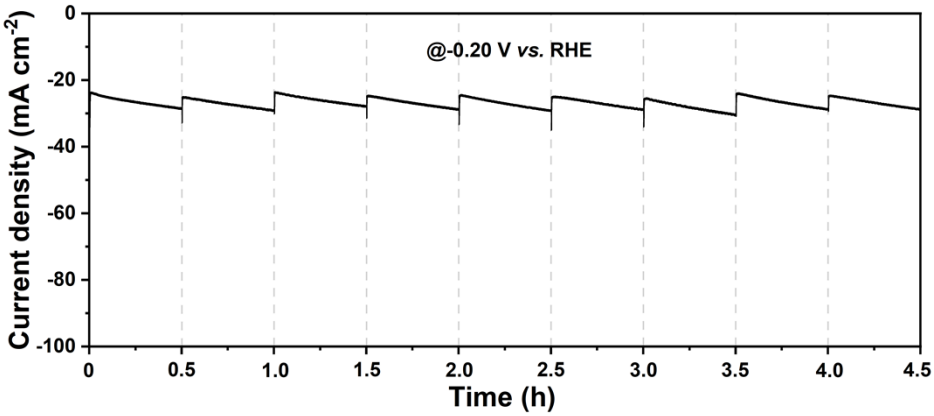

Fig. S13 The current density of cycling tests for FeCoMo/NF at -0.20 V vs. RHE.

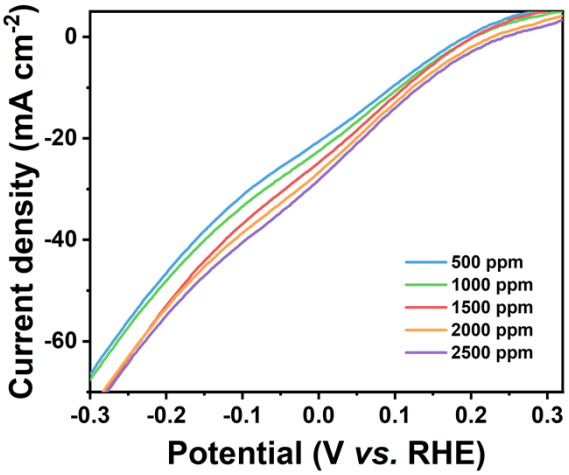

Fig. S14 LSV curves for FeCoMo/NF in 0.1 M KOH with varying NO_3^- concentration.

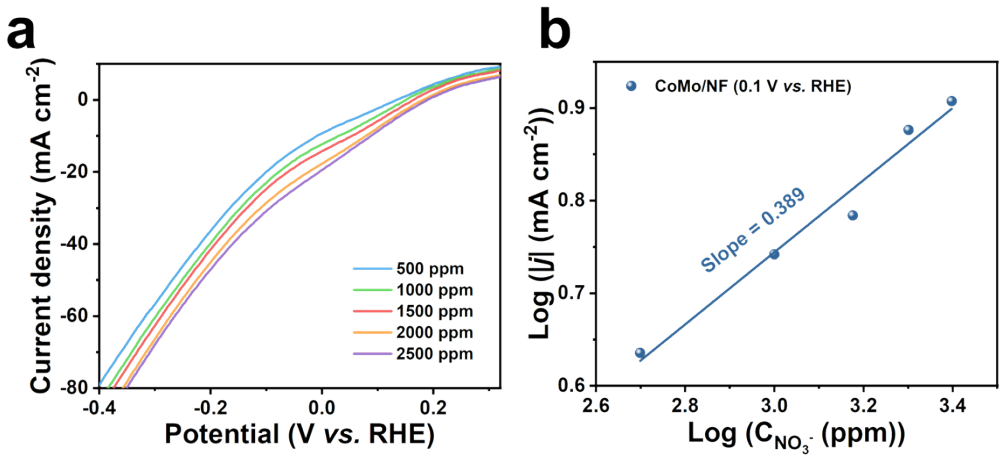

Fig. S15 (a) LSV curves for CoMo/NF in 0.1 M KOH with varying NO_3^- concentration. (b) The logarithm of current density at 0.1 V *vs.* RHE as a function of NO_3^- concentration.

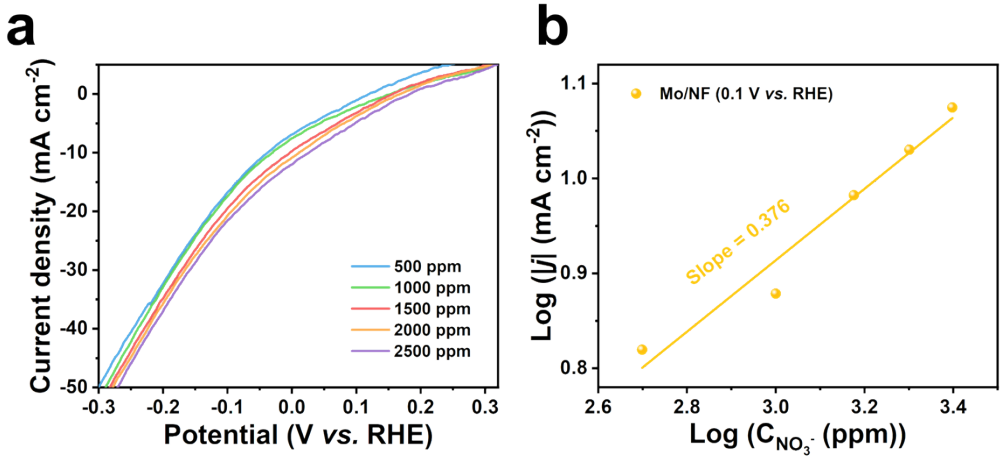

Fig. S16 (a) LSV curves for Mo/NF in 0.1 M KOH with varying NO_3^- concentration. (b) The logarithm of current density at 0.1 V *vs.* RHE as a function of NO_3^- concentration.

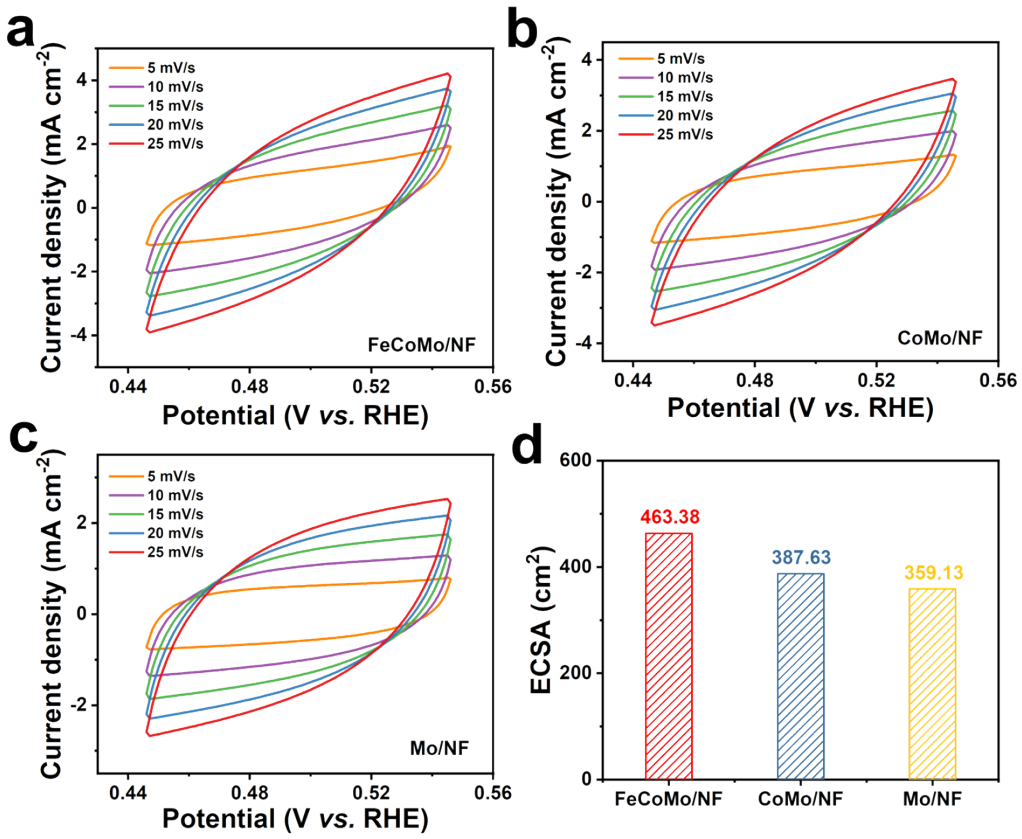

Fig. S17 Electrocatalytic Performance of NO_3RR: CV curves of (a) FeCoMo/NF, (b) CoMo/NF, and (c) Mo/NF. (d) Electrochemical active surface area (ECSA) of FeCoMo/NF, CoMo/NF, and Mo/NF.

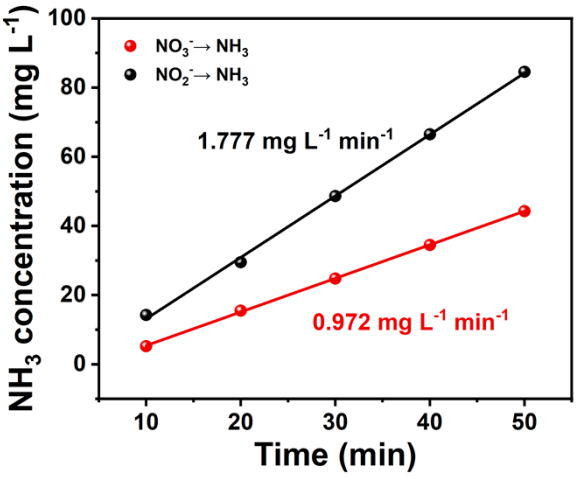

Fig. S18 The conversion rate of NO_3^-→NH_3 and NO_2^-→NH_3 for FeCoMo/NF.

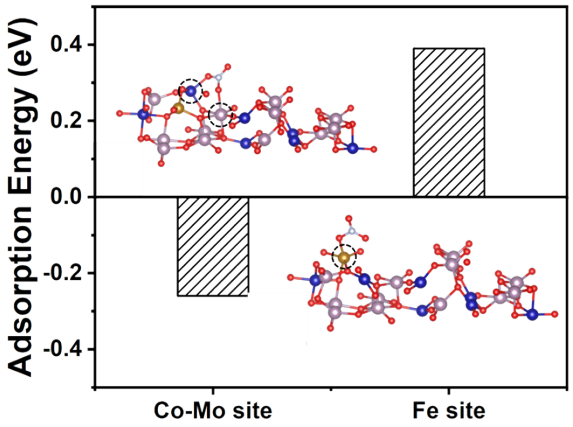

Fig. S19 The adsorption model and adsorption energy of NO_3^- adsorption at Co-Mo and Fe sites.

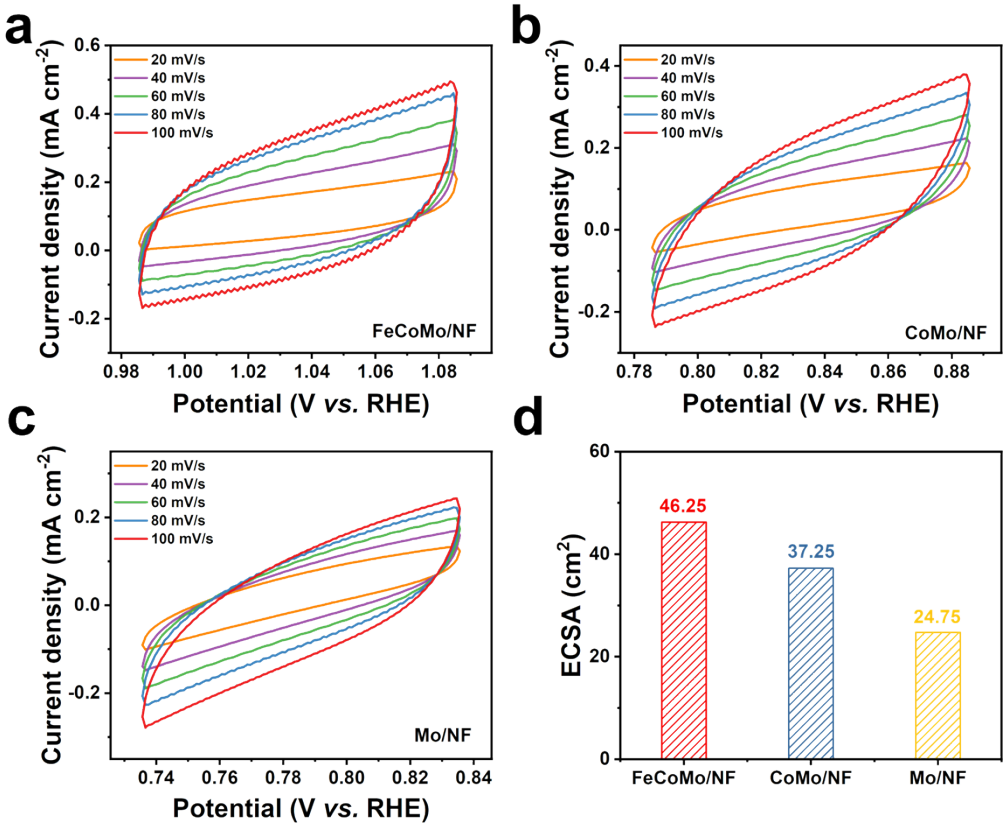

Fig. S20 Electrocatalytic Performance of OER: CV curves of (a) FeCoMo/NF, (b) CoMo/NF, and (c) Mo/NF. (d) Electrochemical active surface area (ECSA) of FeCoMo/NF, CoMo/NF, and Mo/NF.

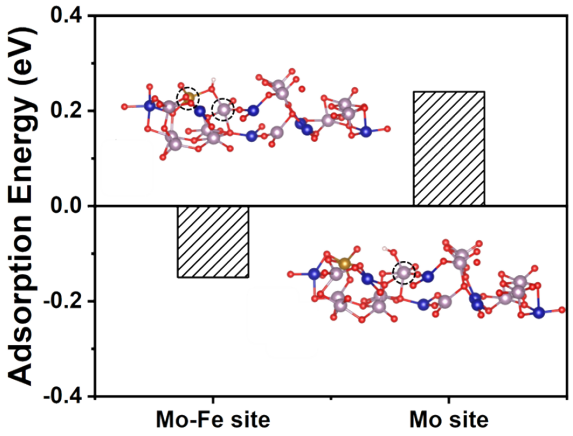

Fig. S21 The adsorption model and adsorption energy of OH^- adsorption at Mo-Fe and Mo sites.

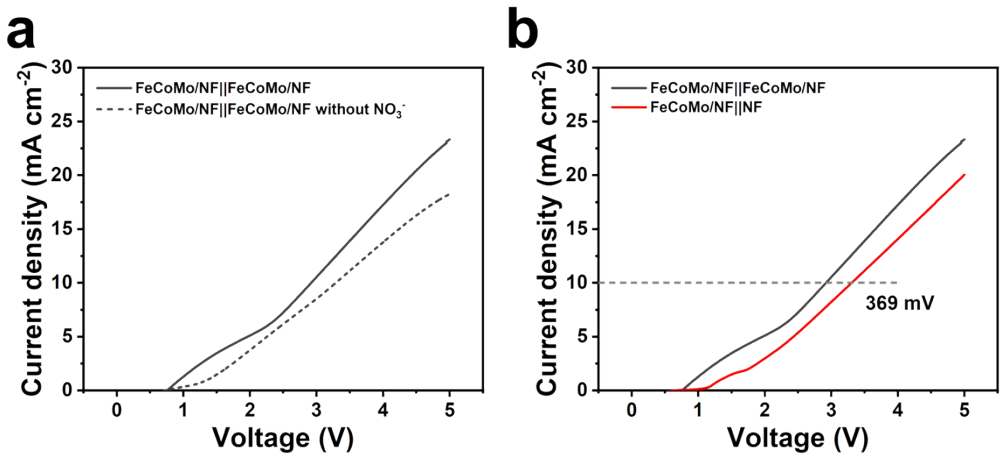

Fig. S22 (a)The LSV curves of the H-type cell in 0.1 M KOH with and without NO_3^-. (b) The LSV curves of FeCoMo/NF||FeCoMo/NF and FeCoMo/NF||NF the H-type cell.

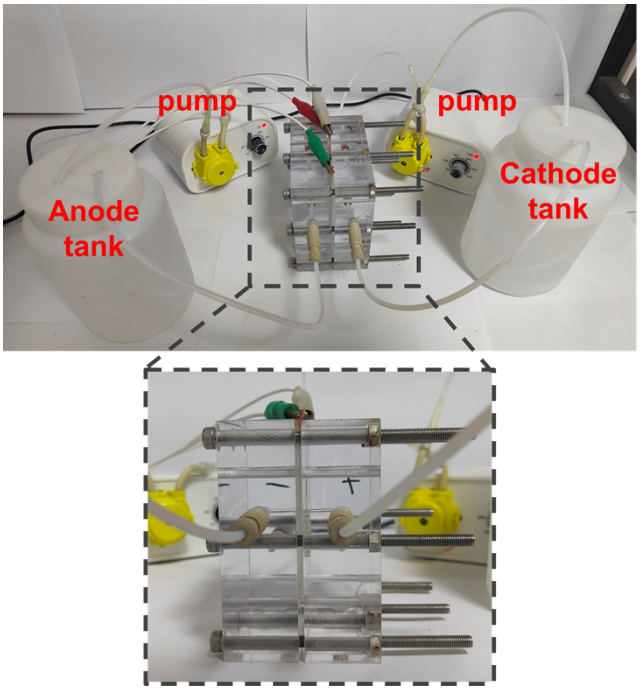

Fig. S23 The flow cell schematic diagram.

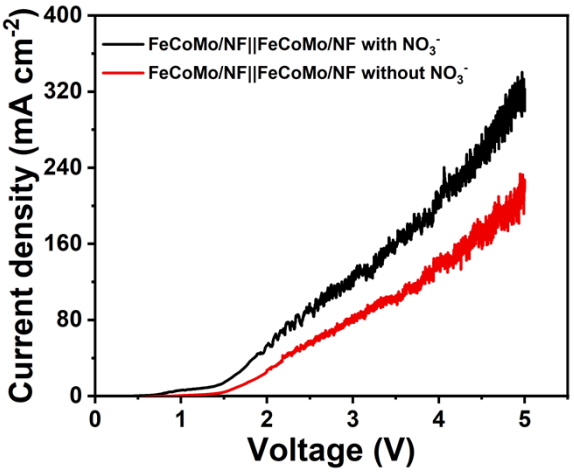

Fig. S24 The LSV curves of the flow cell in 0.1 M KOH with and without NO_3^-.

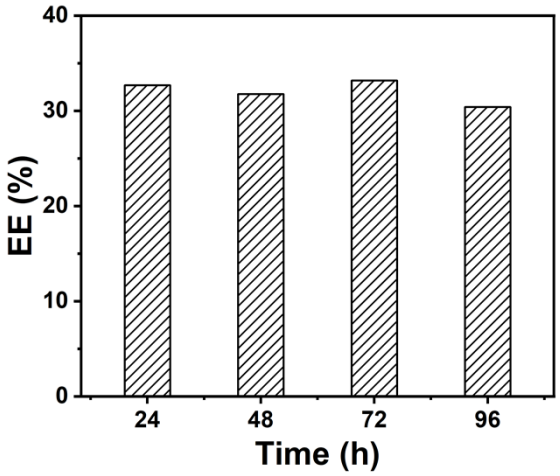

Fig. S25 The EE of FeCoMo/NF||FeCoMo/NF in the flow cell.

Table S1 Comparison of NH_3 yield rate, FE, and potential of recently reported excellent NO_3RR catalysts.

Catalyst	Electrolyte	Potential (*vs.* RHE)	R_{NH3} (mg h^{-1} cm^{-2})	FE (%)	Ref.
FeCoMo/NF	0.1 M KOH+1000 ppm NO_3^-	-0.20 V	2.02	93.43	This work
$CoMn_2O_4$/NC	0.1 M Na_2SO_4+0.1 M $NaNO_3$	-0.70 V	1.04	92.4	[1]
V_{Cu}-Au_1Cu SAAs	0.1 M KOH+7.14 mM KNO_3	-0.20 V	0.56	98.7	[2]
Ru-nanoclusters	1 M KOH+1 M KNO_3	-0.20 V	0.72	100	[3]
FeCoNiAlTi	0.2 M K_2SO_4+50 mM KNO_3	-0.50 V	0.52	95.23	[4]
Fe_1/Cu_2-Co_3O_4	0.2 M Na_2SO_4+100 ppm NO_3^--N	-0.79 V	2.97	98.46	[5]
CoP/CC	1 M NaOH+2 mM $NaNO_3$	-0.40 V	0.32	65	[6]
CMO/NF-800	0.1 M K_2SO_4+1000 ppm NO_3^-	-0.35 V	1.32	94.6	[7]
Co-Fe@Fe_2O_3	0.1 M Na_2SO_4+50 ppm NO_3^--N	-0.75 V	1.51	85.2	[8]

References

1. Niu, Z.; Fan, S.; Li, X.; Duan, J.; Chen, A., Interfacial engineering of $CoMn_2O_4$/NC induced electronic delocalization boosts electrocatalytic nitrogen oxyanions reduction to ammonia. *Applied Catalysis B: Environmental* **2023,** *322*, 122090.

2. Zhang, Y.; Chen, X.; Wang, W.; Yin, L.; Crittenden, J. C., Electrocatalytic nitrate reduction to ammonia on defective Au_1Cu (111) single-atom alloys. *Applied Catalysis B: Environmental* **2022,** *310*, 121346.

3. Li, J.; Zhan, G.; Yang, J.; Quan, F.; Mao, C.; Liu, Y.; Wang, B.; Lei, F.; Li, L.; Chan, A. W. M.; Xu, L.; Shi, Y.; Du, Y.; Hao, W.; Wong, P. K.; Wang, J.; Dou, S.-X.; Zhang, L.; Yu, J. C., Efficient Ammonia Electrosynthesis from Nitrate on Strained Ruthenium Nanoclusters. *Journal of the American Chemical Society* **2020,** *142* (15), 7036-7046.

4. Zhang, R.; Zhang, Y.; Xiao, B.; Zhang, S.; Wang, Y.; Cui, H.; Li, C.; Hou, Y.; Guo, Y.; Yang, T.; Fan, J.; Zhi, C., Phase Engineering of High-Entropy Alloy for Enhanced Electrocatalytic Nitrate Reduction to Ammonia. *Angewandte Chemie International Edition* **2024**, e202407589.

5. Song, M.; Xing, Y.; Li, Y.; Liu, D.; Han, E.; Gao, Y.; Yang, Z.; Yang, X.; He, Y., Fe and Cu Double-Doped Co_3O_4 Nanorod with Abundant Oxygen Vacancies: A High-Rate Electrocatalyst for Tandem Electroreduction of Nitrate to Ammonia. *Inorganic Chemistry* **2023,** *62* (40), 16641-16651.

6. Zhang, H.; Wang, G.; Wang, C.; Liu, Y.; Yang, Y.; Wang, C.; Jiang, W.; Fu, L.; Xu, J., CoP nanowires on carbon cloth for electrocatalytic NOx− reduction to ammonia. *Journal of Electroanalytical Chemistry* **2022,** *910*, 116171.

7. Wang, Y.; Chen, X.; Meng, X.; Li, Z., Joule Heating Synthesis of Cobalt Molybdate with Unsaturated Mo^{4+} Coordination for Greatly Enhanced

Electrocatalytic Nitrate Reduction to Ammonia. *ACS Sustainable Chemistry & Engineering* **2024**, acssuschemeng.4c01335.

8. Zhang, S.; Li, M.; Li, J.; Song, Q.; Liu, X., High-ammonia selective metal–organic framework–derived Co-doped Fe/Fe_2O_3 catalysts for electrochemical nitrate reduction. *Proceedings of the National Academy of Sciences* **2022,** *119* (6), e2115504119.